IOP Publishing Classical and Quantum Gravity
Class. Quantum Grav. **41** (2024) 105011 (22pp) https://doi.org/10.1088/1361-6382/ad3ed9

Spherical warp-based bubble with non–trivial lapse function and its consequences on matter content

G Abellán[1,2,*], **N Bolívar**[1,2] **and I Vasilev**[2]

[1] Departamento de Física, Facultad de Ciencias, Universidad Central de Venezuela, Av. Los Ilustres, Caracas 1041-A, Venezuela
[2] Astrum Drive Technologies, Dallas Pkwy Unit 120 B, Frisco, TX 75034, United States of America

E-mail: gabriel.abellan@ciens.ucv.ve, gabriel@astrumdrive.com, nelson.bolivar@ciens.ucv.ve, nelson@astrumdrive.com and ivaylo@astrumdrive.com

Received 6 May 2023; revised 2 April 2024
Accepted for publication 15 April 2024
Published 26 April 2024

Abstract

In the present work, we study the consequences of including the lapse function as an additional degree of freedom for a general spherical warp-based geometry. By allowing a non-uniform lapse function to evolve, we find that it is possible to accommodate a fluid that includes heat flow. This broadens the range of fluid types that have been studied in these systems and is consistent with the spherical warp metric. Having added the lapse function, we solved the system of equations using an anisotropic fluid with heat flow. In this way, we can examine the different characteristics of the variables of the system. Next, we study the energy conditions and establish how these are modified by including heat flux for an appropriate generic observer in a locally flat spacetime. Finally, we explore all energy conditions using the numerical solutions and verify the regions where they are satisfied.

Keywords: lapse function, heat flux, anisotropy, general relativity, warp bubble

1. Introduction

Since the appearance of the warp drive published by Alcubierre, it is well known that there have been numerous criticisms from several authors, including Alcubierre himself, who already detected some of the problems that this idea would have [1–18]. The main problem has to do

* Author to whom any correspondence should be addressed.

with the need to include exotic matter in order to sustain the spacetime configuration. In this article, we want to explore the possibility of having a warp-based bubble configuration and explore the consequences of including a non-trivial lapse function.

In Cartesian coordinates, the line element according to the ADM formalism [19–21] has the form

$$\mathrm{d}s^2 = -\alpha^2 \mathrm{d}t^2 + (\mathrm{d}x + \beta \mathrm{d}t)^2 + \mathrm{d}y^2 + \mathrm{d}z^2 \,. \tag{1}$$

This kind of line element is widely used and was the starting point for Alcubierre to explore the possibility of warp drives. In his original work, he describes a so called warp bubble moving in a given direction, for instance in (1) describes a 'warping' in the x direction. This bubble obeys very specific constraints regarding the spacetime geometry. Alcubierre assumes in his work that the lapse function $\alpha = 1$ and also proposes a specific form function β. These same assumptions have been incorporated into the vast majority of studies that have been done on the subject.

Recently, some studies on the warp drive configurations have been carried out that do not assume a specific form function and explore in depth the matter content that must be present in order to make the warp drive feasible [22–26]. In the same sense, in previous articles we have explored the use of different symmetries to study a warp–based metric, finding that in this way the analysis of the Einstein equations is much neater. Keeping the geometrical structure of the usual warp bubbles, it is possible to achieve regions where there is flat spacetime separated by a wall which is the boundary of the bubble [27–29]. These investigations have led to a better understanding of the negative energy density problem for warp drives. For example, by working in cylindrical coordinates we have been able to write the Einstein equations in a simple enough form to be able to see that there is a relationship between the energy density and the tangential pressures. In particular, we have found that for dust-like fluids, isotropic fluids, or fluids where the tangential pressures are equal, the energy density is necessarily zero [30]. All these works have in common the interest of studying the complete set of Einstein equations in order to extract constraints and relations between the different degrees of freedom.

As can be seen in (1), the lapse function can be understood as the rate at which the proper time elapses as seen by the Eulerian reference frame. There are several works that analyse how the lapse function influences the general dynamics of the system. For example, in [31], electrodynamics in curved space is analysed using the 3+1 formalism and it is shown that there is a connection between the lapse function and the acceleration felt by an observer whose world line is orthogonal to the spatial 3-surface. In other works such as [32, 33], the relation between the lapse function and thermodynamics is explored.

In this article we aim to examine the consequences of including a general lapse function as an additional degree of freedom to generate a warp-based bubble configuration. For this purpose, in section 2 we will establish the metric and the energy–momentum tensor which we will study and write the Einstein equations for this system. We then include equations of state in order to solve the system and characterise the solutions obtained. Then in section 3 we will examine the energy conditions for this matter configuration and evaluate them using the solutions obtained in the previous section. Finally, we will make some final considerations and discussions in section 4.

2. The spherical warp-based bubble with lapse function

In some recent articles [28, 29], inspired by Alcubierre's metric, we have proposed a line element to describe a warp-based spacetime using spherical coordinates, which is

$$ds^2 = -dt^2 + (dr - \beta dt)^2 + r^2 d\Omega^2 \,, \tag{2}$$

with $d\Omega^2 = d\theta^2 + \sin^2\theta d\phi^2$ and $\beta = \beta(t,r)$ the form function. This line element is based on the ADM formalism, just like Alcubierre's original metric, though there are some differences are worth noting which are important for clarifying what we mean by a warp-based metric. Firstly, the metric for the flat space-like hypersurface has been expressed spherical coordinates instead of Cartesian coordinates. The warp effects of spacetime are still given by the form function β, but correspond to the shift vector in the radial direction. Hence the geometry and dynamics of such a warp bubble are rooted in this function.

A few more comments are in order. Note that Alcubierre's original metric (1) contemplates a positive sign in front of the form function. However, in this work we adopt the convention proposed initially in [22] of inserting a negative sign. Secondly, Alcubierre's original metric, as well as later attempts of generalisation, consider a special combination of coordinates that produce the displacement of the system. For instance, the Alcubierre ansatz can be written in Cartesian coordinates as $\beta = -v_s f(r_s)$, where $r_s^2 = [x - x_s(t)]^2 + y^2 + z^2$. Here it is precisely the function $x_s(t)$ which encodes the displacement of the warp bubble. In a previous work [29], we have considered solutions of this type for the spherical metric (2). It is important to note that we have avoided writing the form function using a coordinate combination of type $r - r_s(t)$ that explicitly describes some kind of displacement. This allows us to focus entirely on the analysis of the warped bubble spacetime, avoiding any effect due to the movement of the centroid of the configuration.

In writing the spherical warp line element, the lapse function has typically been taken to be $\alpha = 1$. We want to examine what happens when we consider a general lapse function. By doing this we obtain a new line element that is given by

$$ds^2 = -\alpha^2 dt^2 + (dr - \beta dt)^2 + r^2 d\Omega^2 \,. \tag{3}$$

Here $\alpha = \alpha(t,r)$ corresponds to the lapse function which is a new degree of freedom of the system. The conditions on functions α, β of the metric have been chosen such that they are consistent with the equations and non–trivial in the inner region, and finally formulating a metric 'warping' in a specific direction. As a final remark on this point, the direction chosen in metric (3) for warping the spacetime is along the radial direction. Due to the spherical symmetry, the resulting metric decreases the number of non-trivial components in the Einstein equation. At the same time, as we have already discussed, the warp bubble configuration is maintained, which is what we intend to study in this work.

Based on the motivations discussed above, the metric (3) does not describe a warp drive, but rather a spherical bubble characterised by a single radial form function. Nevertheless, our metric still retains the imposition on the usual warp drives, as stated in [27], the main imposition being that the matter in the warped region does not exhibit gravitational influence outside of it, the external observer 'sees' only a flat spacetime. Also, the observers inside and outside are timelike, and the tetrads of these observers are equal between them, meaning that the clock rates of observers inside and outside are synchronized, an imposition we relaxed in our present work. As a final remark, we can point out that this line element can be considered in the weak Painlevé–Gullstrand form by taking the 4-vectors $T_a = (-\alpha, 0, 0, 0)$ and $F^a = (0, \beta/\alpha, 0, 0)$ with the following metric factorisation

$$g_{\mu\nu} = (\eta_\alpha)_{ab} \left(\delta_\mu{}^a + T_\mu F^a\right) \left(\delta_\nu{}^b + T_\nu F^b\right) \,, \tag{4}$$

defining $(\eta_\alpha)_{ab} = \mathrm{diag}\{-\alpha^2, 1, r^2, r^2\cos^2\theta\}$.

Using the line element (3) we write in matrix form the metric for the spacetime

$$g_{\mu\nu} = \begin{bmatrix} -\left(\alpha^2-\beta^2\right) & -\beta & 0 & 0 \\ -\beta & 1 & 0 & 0 \\ 0 & 0 & r^2 & 0 \\ 0 & 0 & 0 & r^2\sin^2\theta \end{bmatrix}. \tag{5}$$

Note the off-diagonal terms that are characteristic of the warp-based metric families and the appearance of the lapse function in the g_{00} element.

2.1. Einstein tensor components

Let us now explore the properties of the metric proposed above. For this, we have to consider Einstein's equations

$$G_{\mu\nu} = 8\pi T_{\mu\nu}\,, \tag{6}$$

with $G_{\mu\nu}$ the Einstein tensor and $T_{\mu\nu}$ the energy-momentum tensor. Note that we are working in geometric units where Newton's gravitational constant is $G=1$, and the speed of light is $c=1$. In this way, using the line element (3), the components of the Einstein tensor are

$$\begin{aligned} G_{00} = {} & \frac{\beta}{r^2\alpha^3}\left\{\alpha^3\left(\beta+2r\frac{\partial\beta}{\partial r}\right)+2r\beta^2\left(\beta\frac{\partial\alpha}{\partial r}+\frac{\partial\alpha}{\partial t}\right)-\alpha\beta\left[\beta\left(\beta+2r\frac{\partial\beta}{\partial r}\right)\right.\right. \\ & \left.\left.+2r\left(\alpha\frac{\partial\alpha}{\partial r}+\frac{\partial\beta}{\partial t}\right)\right]\right\}, \end{aligned} \tag{7}$$

$$G_{01} = \frac{\beta}{r^2\alpha^3}\left[-2r\beta\left(\beta\frac{\partial\alpha}{\partial r}+\frac{\partial\alpha}{\partial t}\right)+\alpha\left(\beta^2+2r\beta\frac{\partial\beta}{\partial r}+2r\frac{\partial\beta}{\partial t}\right)\right], \tag{8}$$

$$G_{11} = \frac{1}{r^2\alpha^3}\left[2r\alpha^2\frac{\partial\alpha}{\partial r}+2r\beta\left(\beta\frac{\partial\alpha}{\partial r}+\frac{\partial\alpha}{\partial t}\right)-\alpha\left(\beta^2+2r\beta\frac{\partial\beta}{\partial r}+2r\frac{\partial\beta}{\partial t}\right)\right], \tag{9}$$

$$\begin{aligned} G_{22} = {} & \frac{r}{\alpha^3}\left\{\alpha^2\left(\frac{\partial\alpha}{\partial r}+r\frac{\partial^2\alpha}{\partial r^2}\right)+\left(\beta+r\frac{\partial\beta}{\partial r}\right)\left(\beta\frac{\partial\alpha}{\partial r}+\frac{\partial\alpha}{\partial t}\right)\right. \\ & \left.-\alpha\left[\beta\left(2\frac{\partial\beta}{\partial r}+r\frac{\partial^2\beta}{\partial r^2}\right)+\frac{\partial\beta}{\partial t}+r\left(\frac{\partial\beta}{\partial r}\right)^2+r\frac{\partial^2\beta}{\partial t\partial r}\right]\right\}, \end{aligned} \tag{10}$$

$$\begin{aligned} G_{33} = {} & \frac{r\sin^2\theta}{\alpha^3}\left\{\alpha^2\left(\frac{\partial\alpha}{\partial r}+r\frac{\partial^2\alpha}{\partial r^2}\right)+\left(\beta+r\frac{\partial\beta}{\partial r}\right)\left(\beta\frac{\partial\alpha}{\partial r}+\frac{\partial\alpha}{\partial t}\right)\right. \\ & \left.-\alpha\left[\beta\left(2\frac{\partial\beta}{\partial r}+r\frac{\partial^2\beta}{\partial r^2}\right)+\frac{\partial\beta}{\partial t}+r\left(\frac{\partial\beta}{\partial r}\right)^2+r\frac{\partial^2\beta}{\partial t\partial r}\right]\right\}. \end{aligned} \tag{11}$$

Here, note that we have considered the case where $\beta=\beta(t,r)$ and $\alpha=\alpha(t,r)$. This is reasonable when considering that it is the r-coordinate that could produce shifts in space and not changes in orientation.

2.2. Energy-momentum tensor

In order to write Einstein's field equations we consider an anisotropic fluid with radial heat flux. This is given by

$$T_{\mu\nu} = (\rho+p_\perp)\,u_\mu u_\nu + p_\perp g_{\mu\nu} + (p_r-p_\perp)\,s_\mu s_\nu + u_\mu q_\nu + q_\mu u_\nu\,. \tag{12}$$

with ρ the energy density, p_r the radial pressure, $p_\perp$ the tangential pressure and q the scalar radial heat flux term. For writing this expression, we have considered the following four vectors

$$u_\mu = (-\alpha, 0, 0, 0) \ , \qquad s_\mu = (-\beta, 1, 0, 0) \ , \qquad q_\mu = q s_\mu \ . \tag{13}$$

Here u_μ is time–like and corresponds to an observer that moves along directions normal to the spatial slices following geodesic curves, that is with zero acceleration, usually known as Eulerian observers. On the other hand, s_μ and q_μ are space–like. These vectors satisfy the relations $u^\mu u_\mu = -1$, $s^\mu s_\mu = 1$, $q^\mu q_\mu = q^2$, $u^\mu s_\mu = u^\mu q_\mu = 0$.

Using the parametrization (13), we write the energy–momentum tensor in matrix form

$$T_{\mu\nu} = \begin{bmatrix} \alpha^2\rho + \beta^2 p_r + 2\alpha\beta q & -(\beta p_r + \alpha q) & 0 & 0 \\ -(\beta p_r + \alpha q) & p_r & 0 & 0 \\ 0 & 0 & r^2 p_\perp & 0 \\ 0 & 0 & 0 & r^2 \sin^2\theta\, p_\perp \end{bmatrix} . \tag{14}$$

It is important to remark that from the (10) and (11) components of the Einstein tensor and the momentum energy tensor, both components of the tangential pressure must be equal. This is a consequence of the spherical symmetry of the metric.

Another aspect that is important to consider is that from equation (6) and knowing that $u^\mu = (\alpha^{-1}, \alpha^{-1}\beta, 0, 0)$ we obtain the following relation

$$\begin{aligned} T_{\mu\nu}u^\mu u^\nu &= \frac{1}{8\pi} G_{\mu\nu}u^\mu u^\nu \\ &= \frac{1}{8\pi}\left(G_{00} + 2\beta G_{01} + \beta^2 G_{11}\right) \\ &= \frac{\beta}{8\pi r^2\alpha^2}\left(\beta + 2r\frac{\partial\beta}{\partial r}\right). \end{aligned} \tag{15}$$

But we also have the relation for energy density $T_{\mu\nu}u^\mu u^\nu = \rho$, thus we could write

$$\rho = \frac{\beta}{8\pi r^2\alpha^2}\left(\beta + 2r\frac{\partial\beta}{\partial r}\right) . \tag{16}$$

This expression corresponds to the energy density as seen by the Eulerian observer.

Using the following combinations of the Einstein tensor, $G_{01} + \beta G_{11}$, $G_{00} + 2\beta G_{01} + \beta^2 G_{11}$, G_{11} and $G_{22} - r^2 G_{11}$, and the respective $T_{\mu\nu}$ combination we can write a suitably simplified version of the field equations, which are explicitly

$$-\frac{\beta}{4\pi r\alpha^2}\frac{\partial\alpha}{\partial r} = q \ , \tag{17}$$

$$\frac{\beta}{8\pi r^2\alpha^2}\left(\beta + 2r\frac{\partial\beta}{\partial r}\right) = \rho \ , \tag{18}$$

$$\frac{1}{8\pi r^2\alpha^3}\left[2r\alpha^2\frac{\partial\alpha}{\partial r} + 2r\beta\left(\beta\frac{\partial\alpha}{\partial r} + \frac{\partial\alpha}{\partial t}\right) - \alpha\left(\beta^2 + 2r\beta\frac{\partial\beta}{\partial r} + 2r\frac{\partial\beta}{\partial t}\right)\right] = p_r \ , \tag{19}$$

$$\begin{aligned} &\frac{1}{8\pi r^2\alpha^3}\left\{r\alpha^2\left(-\frac{\partial\alpha}{\partial r} + r\frac{\partial^2\alpha}{\partial r^2}\right) + r\left(-\beta + r\frac{\partial\beta}{\partial r}\right)\left(\beta\frac{\partial\alpha}{\partial r} + \frac{\partial\alpha}{\partial t}\right)\right. \\ &\quad \left. + \alpha\left[\beta\left(\beta - r^2\frac{\partial^2\beta}{\partial r^2}\right) + r\left(\frac{\partial\beta}{\partial t} - r\left(\frac{\partial\beta}{\partial r}\right)^2 - r\frac{\partial^2\beta}{\partial t\partial r}\right)\right]\right\} = \Delta \ . \end{aligned} \tag{20}$$

Here $\Delta = p_\perp - p_r$ corresponds to the anisotropy factor. These expressions correspond to time–dependent anisotropic warp–bubble with non–trivial lapse function. This system has in general 6 degrees of freedom: $\alpha, \beta, \rho, p_r, \Delta, q$. Therefore we need to provide two additional conditions in order to close the system.

It is important to note that the lapse function affects all material variables. In particular, we note that the radial heat flux depends directly on the gradient of the lapse function in the radial direction (17). Therefore, if $\alpha = 1$, it is not possible to have a metric like (2) which also has heat flux.

As mentioned above, it is necessary to provide two additional relations in order to solve the system of equations (17)–(20). Here we use a simple model for radial pressure and anisotropy factor

$$p_r = K_r\,(\rho - \lambda)\ , \tag{21}$$

$$\Delta = K_\Delta\,(\rho - \rho_0)\ , \tag{22}$$

with λ, K_r, K_Δ appropriate real constants and ρ_0 the density at the center $r = 0$ of the bubble. This ensures the correct behaviour of the anisotropy factor Δ at the origin [34]. These equations are inspired by MIT bag models applied to astrophysical systems [35]. The choice of a linear model for the equations of state allows us to explore a simple yet non-trivial model that produces an interesting behaviour of the physical quantities under study. All free parameters provide enough flexibility to eventually modify the behaviour of the system in simulations and even modelling aspects that can be subjected to experimentation.

After providing the equations of state, it is also necessary to specify initial and boundary conditions. A careful analysis of the system of equations allows us to derive that a consistent set of conditions is given by

$$\alpha\,(0,r) = 1.0\ , \tag{23}$$

$$\beta\,(0,r) = \beta_0\, r^2\,(30 - r)^2 \exp\left[-\frac{(r-15.0)^2}{30.0}\right]\ , \tag{24}$$

$$\alpha\,(t,0) = 1\ , \qquad \frac{\partial \alpha}{\partial r}\,(t,30) = 0\ ; \qquad \beta\,(t,0) = \beta\,(t,30) = 0\ . \tag{25}$$

The initial and boundary conditions for β are chosen to allow us modelling the evolution of a localised perturbation when there is no perturbation at the borders. The initial value for β is not entirely Gaussian due to the polynomial factor and has been chosen for simplicity, both in the model and the numerical calculations. Moreover, we have chosen as initial lapse function $\alpha(0,r) = 1$ to the one that does not differ from the standard case that corresponds with no dissipation. The boundaries are set in order to have a truncated spacetime, flat inside and outside the warped region.

It is worth mentioning that due to the results of the numerical simulation, $\rho_0 = 0$ must be fulfilled. Another value would be inconsistent. This can be derived from equation (16), where it follows that $\beta(t,0) = 0$ directly implies that the energy density vanishes in the center for all t. Moreover, we have that $\beta(t,0) = 0$ is a consequence of the initial condition (24) and the dynamics. The rest of the parameters (β_0, K_r, K_Δ, λ) have been set so that the numerical simulation converges in a reasonable time.

2.3. Numerical results

The objective of the simulation is to make a first assessment of the evolution of the system using a robust known numerical method. The numerical simulations were implemented using PETSc [36–39]. We employed a discretization process, finite difference (FD), and simplified the equations. Consistency was checked by calculating the difference between the FD and the exact forms. To solve the system, we used a backward differentiation formula of order $= 1$ and an implicit scheme, corresponding to the backward Euler method, as implemented in the PETSc package. Then, using the method of lines (MOL), we eliminated the spatial component and solved a system of ODEs for time. This method approximates the derivative for a given function and time using results from already computed time points, thereby increasing the accuracy of the approximation.

The stability was studied, and the global error was estimated to be bounded. Further, we made a Taylor expansion of the first and second-order derivatives and checked consistency when Δr and Δt tend to zero. The global error can be estimated to be of the form $e^{n+1} = ||A^{-1}(x^{n+1})[A(x^{n+1})(x_{ex}^{n+1} - x^{n+1})]||$ at each step n, where e is the global error function, and x, F, and A are vectors and matrices of size dependent on the number of spatial points N. From the above, we can prove that the error is $e^{n+1} \leqslant \exp(T_f a)e^0 + \exp(T_f a)\frac{Mh}{2a}$, where M is proportional to the exact second derivative of x, and a is a bounded quantity. Because the global error $e^0 = 0$, when the step time h goes to zero, the error is bounded, and the solutions are more stable (see details in appendix). Since the numerical method is standard and furthermore this work does not attempt to evaluate the effectiveness of the implemented numerical scheme, we consider that it is beyond our scope to go further into the nature of the numerical method used. In general, we do not expect a certain behaviour of the system, but only an estimation of how the evolution suggests to go in the specified interval and using the selected numerical methods. It seems, at least given the computational power and the time range considered, that the system does not reach a steady state.

In figure 1 we depicted the form function β, lapse function α, and heat q as a function of r for both isotropic and anisotropic systems. We have considered several time values for solutions. As a general feature it can be seen that the form function β is formed by a bump which barely changes between the isotropic and anisotropic cases. The changes can be seen mainly around the centre of the plot.

The lapse function α has extreme points with maxima and minima. We also note that at no time does a change of signature occur, although there are regions where $\alpha < 1$ is observed. Non-uniform α implies that time flows with different rates for the same observer at different positions. This is a signature of local gravitational effects on the observer as it evolves over different hypersurfaces.

Finally, the heat flow q presents a similar behaviour in both cases, the most outstanding characteristic being the fact that there are regions with positive heat flow and others with negative heat flow.

It is interesting to study the relation between the form function β and the heat flux q, with the lapse function α. In order to do this we plot both quantities using the coordinate r as the implicit variable, that means correlating each of the values of α at the domain r with the value of β and q in the same r domain point. In figure 2, it can be seen for an anisotropic fluid that the form function and lapse function constitute a bounded map. This might suggest that physical behaviour is reasonable since the values of these degrees of freedom do not diverge. It is clear that the heat flux reaches larger amplitudes along with the lapse function and then contracts.

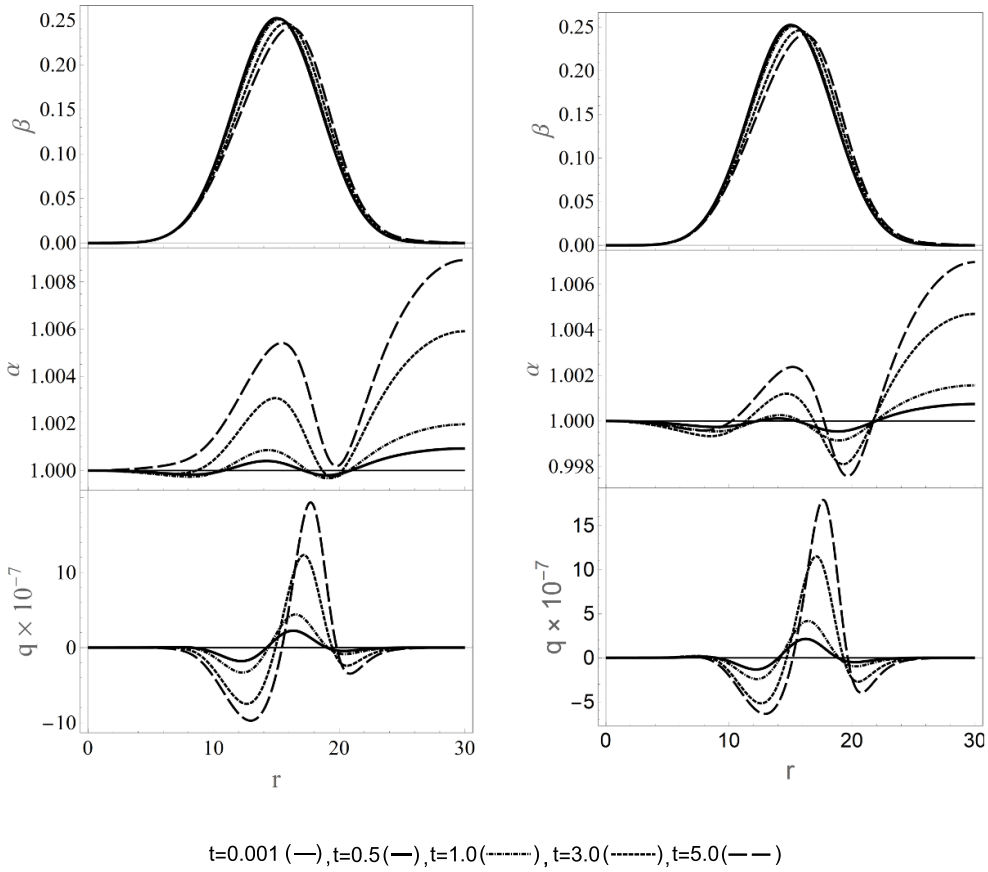

Figure 1. The plot shows the β function, lapse function α and heat flux q as a function of the radial coordinate r without anisotropy $\Delta = 0$ (left) and with anisotropy $\Delta \neq 0$ (right). Parameters used $\beta_0 = 5 \times 10^{-6}$, $\lambda = 0$, $K_r = 0.01$, $K_\Delta = 0.01$ (only for anisotropic case).

Similarly, for increasing times, the path of the map becomes wider, reaching higher values of α and q. Also seen in this figure on the right–hand side is the equation of state between radial pressure and energy density, which shows a linear relation and was modeled using a bag-like model pointing to a modified ideal gas equation.

Next, we have in figure 3 (left) the anisotropy factor Δ, the energy density ρ, and the radial pressure p_r in terms of the lapse function α using r as an implicit parameter. It can be seen that they constitute bounded maps and, as in figure 2, the shape of the plots seems to expand for increasing times. This is due to the fact that the evolution of the lapse function departs from $\alpha \to 1$ as time evolves. As can be expected, the three plots are similar due to the equations of state used (21) and (22), the only change being the scale associated with each physical variable.

Finally, in figure 4(a) contour map is shown relating the thermodynamical variables, radial pressure p_r, heat flux q, and energy density ρ. This plot is parameterised by the energy density. In general there is no unique correlation with the signs of the physical quantities. However, it

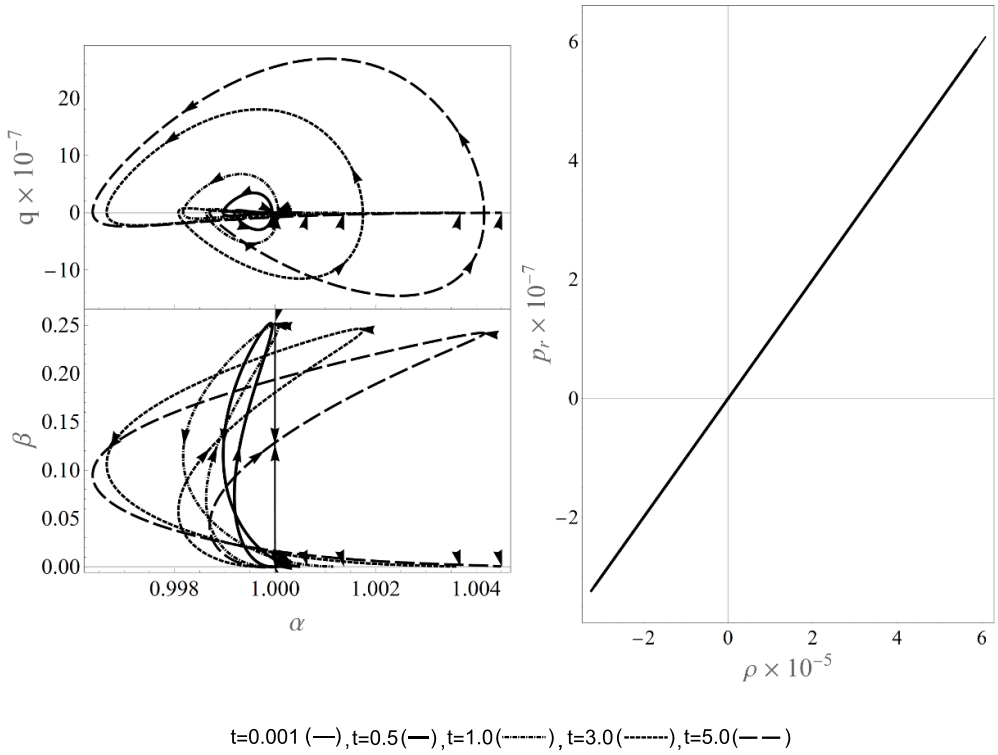

Figure 2. The left plot shows the heat q and the function β and its dependence with α (r implicit) for an anisotropic fluid. The parameters values are $\beta_0 = 5 \times 10^{-6}$, $K_r = 0.01$, $K_\Delta = 0.01$, $\lambda = 0$.

can be noted that for radial pressures and energy densities greater than zero, there is a large region with positive heat flux and only a thin zone where it is negative. Similarly, a predominance of positive heat flux is observed when the radial pressure and energy density are negative. This process is a consequence of the lapse function deviating from its standard value $\alpha = 1$. On the other hand, figure 5 offers a different perspective of the relation between the three variables, showing the linear character of the energy density and the radial pressure and the non-trivial correlation between the energy density and the heat flux.

3. Energy conditions

Energy conditions are expressions that can be used to relate the quantities that appear in the energy-momentum tensor $T_{\mu\nu}$. As is well known, these expressions are used more as a rough guideline than as a constraint on these quantities. It is convenient to examine these conditions in order to have some understanding of the behaviour of the material sector of the theory and to be able to control non–physical aspects of the system [20, 40–44]. In the following we will evaluate, as usual, the energy conditions for an appropriate generic observer and we will see how these conditions are changed by including heat flow as part of the system.

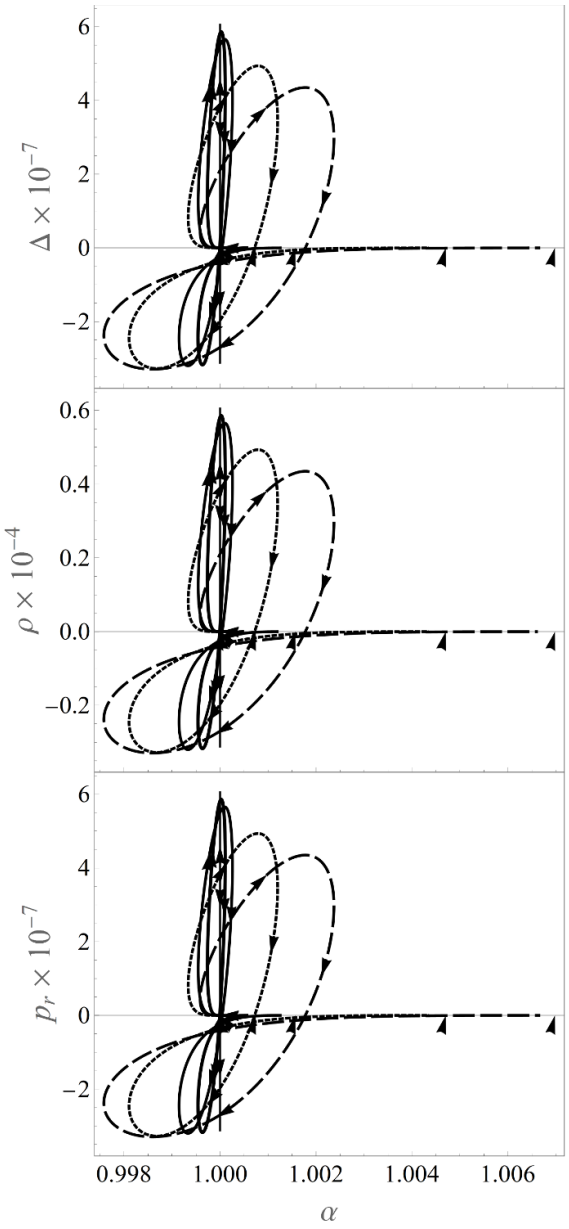

Figure 3. Plots (r implicit) between the matter quantities and the lapse function for an anisotropic fluid. Parameters values $\beta_0 = 5 \times 10^{-6}$, $K_r = 0.01$, $K_\Delta = 0.01$, $\lambda = 0$.

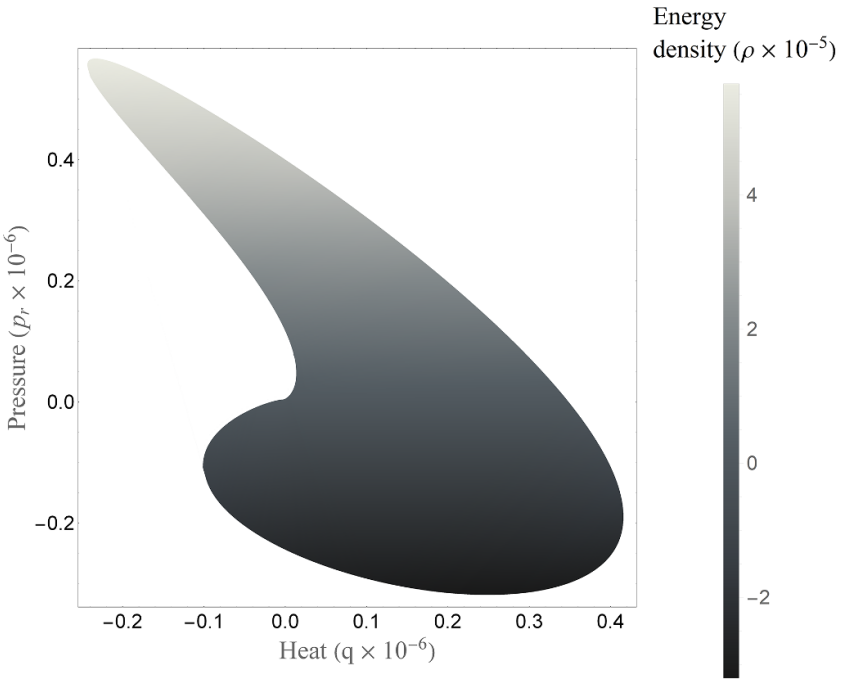

Figure 4. Density plot showing the linearly interpolated correlations between the matter heat, radial pressure, and energy density for $t = 5.0$. Parameters values $\beta_0 = 5 \times 10^{-6}$, $K_r = 0.01, K_\Delta = 0.01, \lambda = 0$. The grey tones region shows the interpolation between the three variables. The physical points correspond to the boundary of the plot; the shaded inner region shows the energy density values at these points.

In order to examine the energy conditions, it is convenient to move to a local Minkowskian frame in such a way that $g_{\mu\nu} = e^{\hat{\alpha}}{}_{\mu} e^{\hat{\beta}}{}_{\nu} \eta_{\hat{\alpha}\hat{\beta}}$ is satisfied with $\eta_{\hat{\alpha}\hat{\beta}} = \text{diag}\{-1,1,1,1\}$. For this, we use the following change of basis

$$e^{\hat{0}}{}_{\mu} = (-\alpha, 0, 0, 0)\,, \tag{26}$$

$$e^{\hat{1}}{}_{\mu} = (-\beta, 1, 0, 0)\,, \tag{27}$$

$$e^{\hat{2}}{}_{\mu} = (0, 0, r, 0)\,, \tag{28}$$

$$e^{\hat{3}}{}_{\mu} = (0, 0, 0, r\sin\theta)\,. \tag{29}$$

Here the indices with hats belong to the local Minkowskian spacetime and the indices without hats correspond to the global spacetime. In this local frame, the energy–momentum tensor (12) is written as

$$T_{\hat{\alpha}\hat{\beta}} = (\rho + p_\perp) u_{\hat{\alpha}} u_{\hat{\beta}} + p_\perp \eta_{\hat{\alpha}\hat{\beta}} + (p_r - p_\perp) s_{\hat{\alpha}} s_{\hat{\beta}} + u_{\hat{\alpha}} q_{\hat{\beta}} + q_{\hat{\alpha}} u_{\hat{\beta}}\,, \tag{30}$$

with the following 4–vectors

$$u_{\hat{\alpha}} = (-1, 0, 0, 0)\,, \qquad s_{\hat{\alpha}} = (0, 1, 0, 0)\,, \qquad q_{\hat{\alpha}} = q s_{\hat{\alpha}}\,. \tag{31}$$

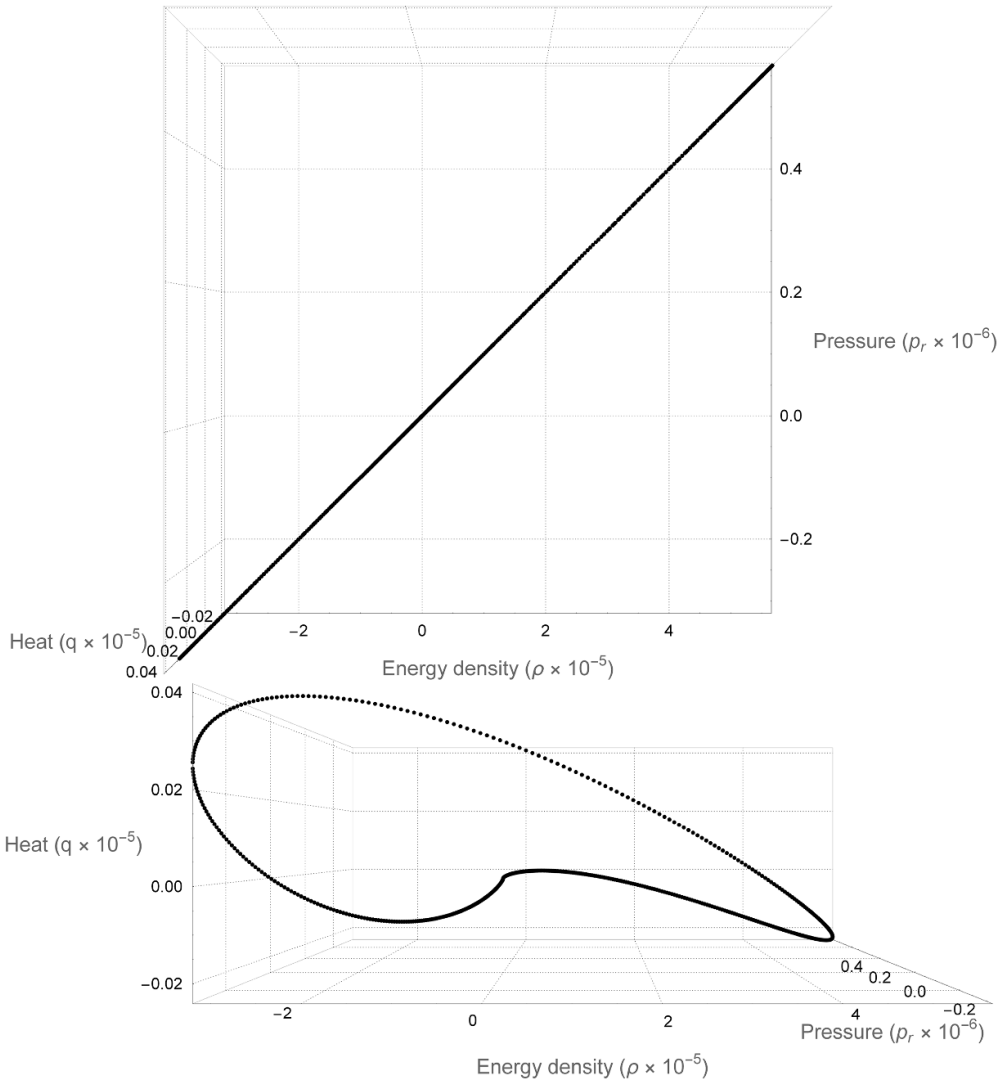

Figure 5. 3D plot showing the correlations between the matter heat, radial pressure, and energy density for $t = 5.0$. The above view shows the linear relation between energy density and the radial pressure. The front view depicts show us the parameter path followed by changes in the heat. Parameters values are $\beta_0 = 5 \times 10^{-6}$, $K_r = 0.01$, $K_\Delta = 0.01$, $\lambda = 0$.

In matrix form, the energy–momentum tensor is written as

$$T_{\hat{\alpha}\hat{\beta}} = \begin{bmatrix} \rho & -q & 0 & 0 \\ -q & p_r & 0 & 0 \\ 0 & 0 & p_\perp & 0 \\ 0 & 0 & 0 & p_\perp \end{bmatrix}, \tag{32}$$

which can be clearly recognised as describing an anisotropic fluid with radial heat flux.

In order to study the energy conditions for a generic observer with respect to the local frame we consider the following generic 4-vectors

$$v^{\hat{\alpha}} = \gamma\,(1,a,b,c)\ , \qquad \text{with} \qquad a^2+b^2+c^2<1\ , \tag{33}$$

$$k^{\hat{\alpha}} = (1,a',b',c')\ , \qquad \text{with} \qquad a'^2+b'^2+c'^2=1\ , \tag{34}$$

with $\gamma=(1-a^2-b^2-c^2)^{-1/2}$. It is clear that $v^{\hat{\alpha}}$ and $k^{\hat{\alpha}}$ correspond to 4-vectors of time and null kind respectively. These expressions allow us to describe generic observers adapted to the type of condition we are studying. In the case of the weak, strong and dominant conditions the generic observer is described by (33) while in the null condition the observer is given by (34). Now, using all these settings, we move on to study the energy conditions. For this we follow an optimisation scheme using Lagrange multipliers and finding all the allowed solutions.

3.1. Weak energy condition (WEC)

This requires that $T_{\hat{\alpha}\hat{\beta}}v^{\hat{\alpha}}v^{\hat{\beta}}\geqslant 0$ for a generic future-pointing timelike vector (33). We find that

$$\rho\geqslant 0\,, \tag{35}$$

$$\rho+p_r-2q>0\,, \tag{36}$$

$$\rho+p_\perp>0\,, \tag{37}$$

$$\rho+p_\perp-\frac{q^2}{p_r-p_\perp}>0\,. \tag{38}$$

So the WEC is satisfied for any observer in the local frame if each of the above inequalities is satisfied. We see that this condition is affected by the inclusion of heat flux. From plots (a), (c), (d) and (e) in figure 6, we can see that the weak condition is not satisfied for any instant in the studied domain.

3.2. Strong energy condition (SEC)

The SEC imposes a bound on the Ricci tensor $R_{\mu\nu}$ which yields an evaluation of the following expression

$$\left(T_{\hat{\alpha}\hat{\beta}}-\frac{1}{2}T\eta_{\hat{\alpha}\hat{\beta}}\right)v^{\hat{\alpha}}v^{\hat{\beta}}\geqslant 0\,. \tag{39}$$

The following relations follow from this expression

$$\rho+p_r+2p_\perp>0\,, \tag{40}$$

$$\rho+p_r-2q>0\,, \tag{41}$$

$$\rho+p_\perp>0\,, \tag{42}$$

$$\rho+p_\perp-\frac{q^2}{p_r-p_\perp}>0\,. \tag{43}$$

Note the dependence on heat flow. From plots (b), (c), (d) and (e) in figure 6, we can see that the strong condition is not satisfied for any instant in the studied domain.

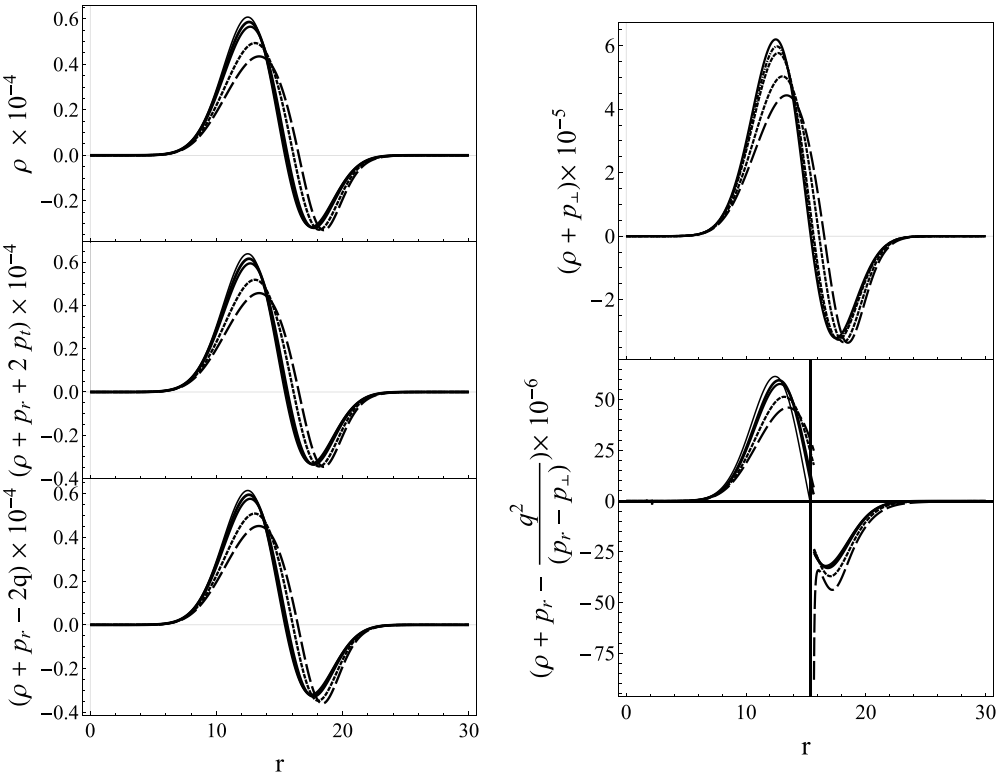

Figure 6. Plots for WEC, SEC, NEC conditions. Parameters values $\beta_0 = 5 \times 10^{-6}$, $K_r = 0.01$, $K_\Delta = 0.01$, $\lambda = 0$.

3.3. Null energy condition (NEC)

The NEC $T_{\hat{\alpha}\hat{\beta}} k^{\hat{\alpha}} k^{\hat{\beta}} \geqslant 0$ is analogous to weak condition but with null vector $k^{\hat{\alpha}}$ replacing the time vector $v^{\hat{\alpha}}$. This time, using (34) we obtain

$$\rho + p_r - 2q \geqslant 0\,, \tag{44}$$

$$\rho + p_\perp \geqslant 0\,, \tag{45}$$

$$\rho + p_\perp - \frac{q^2}{p_r - p_\perp} \geqslant 0\,. \tag{46}$$

Here we have used condition $a'^2 + b'^2 + c'^2 = 1$. The NEC includes a contribution both from the heat flux and tangential pressure. From plots (c), (d) and (e) in figure 6, we can see that the null condition is not satisfied for any instant in the studied domain.

3.4. Dominant energy condition (DEC)

In this case, it is required that the expression $F^{\hat{\alpha}} = T^{\hat{\alpha}}{}_{\hat{\beta}} v^{\hat{\beta}}$ is a future-pointing causal vector. So that $F^{\hat{\alpha}} F_{\hat{\alpha}} \leqslant 0$ is fulfilled.

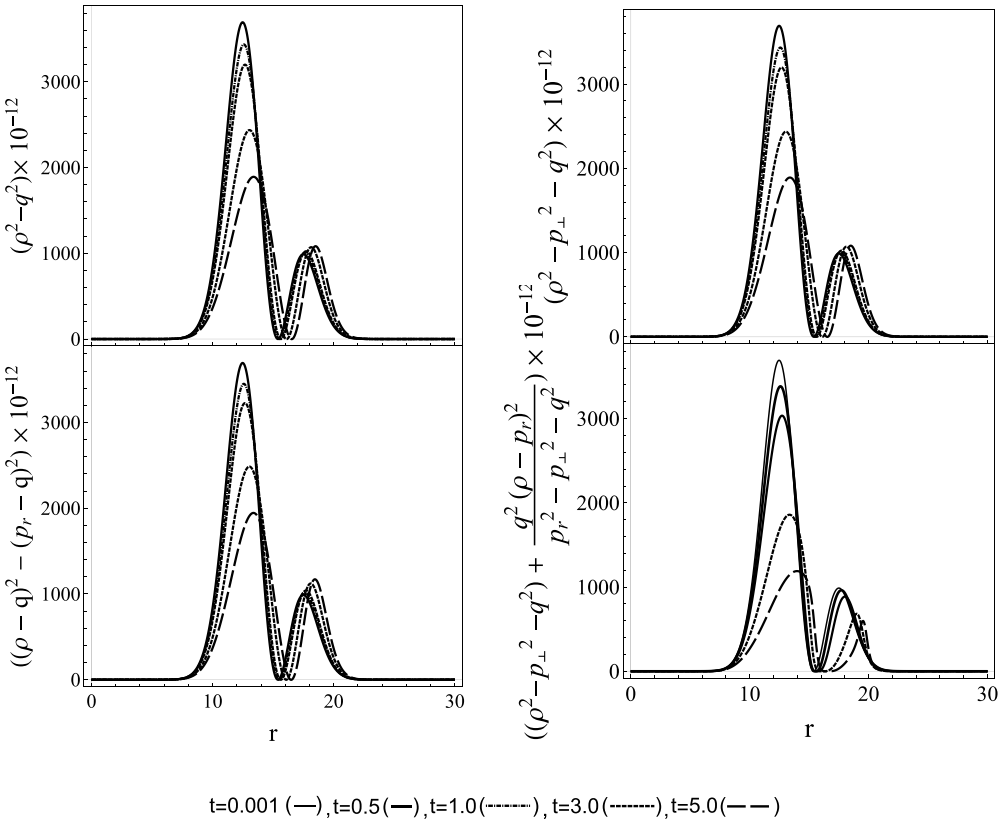

Figure 7. Plots for DEC condition. Parameters values $\beta_0 = 5\times 10^{-6}$, $K_r = 0.01$, $K_\Delta = 0.01$, $\lambda = 0$.

Using (32) and (33), and after some straightforward calculations, we find that $F^{\hat{\alpha}}F_{\hat{\alpha}} = T^{\hat{\alpha}}{}_{\hat{\beta}}T_{\hat{\alpha}\hat{\gamma}}v^{\hat{\beta}}v^{\hat{\gamma}} = -\gamma^2(\rho-aq)^2+\gamma^2(ap_r-q)^2+\gamma^2b^2p_\perp^2+\gamma^2c^2p_\perp^2$. So we obtain the following expressions

$$\rho^2-q^2 \geqslant 0\,, \tag{47}$$

$$(\rho-q)^2-(p_r-q)^2>0\,, \tag{48}$$

$$\rho^2-p_\perp^2-q^2>0\,, \tag{49}$$

$$\rho^2-p_\perp^2-q^2+\frac{q^2(\rho-p_r)^2}{p_r^2-p_\perp^2-q^2}>0\,. \tag{50}$$

where we have used the condition $a^2+b^2+c^2<1$. Note the appearance of heat flow in this expression. What we find is that heat flow cannot dominate all other physical variables. In this case, we see that plots (a), (b), (c), and (d) in figure 7 show that the DEC is satisfied.

It is important to note that for the WEC, SEC and NEC conditions the plot (e) in figure 6 shows a singularity because the anisotropy vanishes at that point. The expressions (38), (50) are obtained by considering an observer with arbitrary time and null 4–velocity respectively, and are expressions that are rarely reported in the literature. As can be noted in plot (a) of

figure 6, the energy conditions are dominated by the energy density. It is also observed that, while there are regions of the domain in r where the conditions are satisfied, this is in general not true for the entire domain for all energy conditions. It is interesting to note that the DEC is satisfied in the whole domain and for every instant t.

Finally, it is interesting to note that the energy-momentum tensor examined (32) could be labelled as type I according to the [45] classification. An energy–momentum tensor of type I has a timelike eigenvector and in our case it occurs as long as condition $\rho + p_r - 2q > 0$ is satisfied. This expression appears in each and every energy condition shown above, even in the DEC, although it is not obvious, since $(\rho - q)^2 - (p_r - q)^2 = (\rho - p_r)(\rho + p_r - 2q)$. An in-depth review of this type of matter content can be seen in [46] and more recently [47, 48]. For an extended review of the Hawking–Ellis classification see [49] and the references therein.

4. Final remarks

In this work, we have analysed the effect of considering a lapse function α as an additional degree of freedom on a spherical line element describing a warp-based bubble in spherical coordinates, which itself is characterised by the form function β. The objective has been to understand the consequences on the material content of the system after including a spherically symmetric general lapse function. This can be useful by itself either for modelling some kind of phenomenology or from a purely theoretical perspective.

As we have shown in previous work [30], spherical symmetry allows us to find a neater system of equations, eliminating the redundant relations from Einstein equations of warp–like systems. This is particularly useful when dealing with problems involving material distributions, where one can clearly read the links with matter and the energy conditions involved.

The main result of this work is that for the proposed line element and considering a general lapse function of the form $\alpha(t, r)$, we have been able to include the heat flux in the energy–momentum tensor.

It can be seen from writing the Einstein equations that there is a direct dependence between the lapse function and the heat flux. For instance, it is evident that by making the lapse function independent of the radial coordinate, the heat flux disappears. This fact includes the trivial and extensively studied case in the 3+1 formalism where $\alpha = 1$. However, it leaves open the possibility for a non-trivial uniform lapse function which is a function only of the time coordinate.

Since the lapse function is related to how observers measure the time dilation and since we have seen that the heat flux is related to the spatial derivatives of the lapse function, we can conclude that there is a correlation between the rate of flow in the clocks of different observers and the heat flux. We also note that the proposed metric shares some resemblance with the Gödel metric and it is well–known that this metric admits closed time–like curves [45, 50]. This is beyond the scope of the present work but we believe it is worth exploring these aspects in future research.

To solve the system it was necessary to indicate additional conditions. We choose a linear model as the equation of state for both radial pressure and anisotropy. Such equations are common and their phenomenology is that of the classical ideal gas and is well known. When solving, we note that qualitatively there is no large difference between the isotropic and the anisotropic system (see figure 1). We have found that the Einstein equations allow the evolution of the lapse function in a non-trivial way, with the heat flux being related to the spatial gradient of the lapse function. We have also mapped the main physical variables in terms of the lapse function, finding in all cases that the functions are well-behaved (figures 2 and 3). In all of

the cases, as time evolves, the physical quantities present an expanding behaviour from the lapse function value $\alpha = 1$. We find interesting the contour plot relating ρ, p_r, and q, which gives an idea of the interplay between the three main thermodynamic variables (figure 4). We have found large regions where there is almost no heat flow, with the maximum and minimum values corresponding to a non-trivial point of intermediate energy density and radial pressure.

We then reviewed the weak, strong, null and DECs, from which we have been able to extract constraints for the components of the energy-momentum tensor and therefore relations for matter that would enable this spacetime to be supported. We have performed the full analysis by switching to a local Minkowskian observer and then introducing time and null-type generic vectors to describe any observer with respect to the local frame. In order to achieve the results, a simple optimisation scheme was carried out and additional expressions were obtained which are not usually reported in the literature. What we have found is that only the DEC is satisfied while the weak, null, and strong conditions are not. Nonetheless, there are regions of the domain in r where all the conditions can be said to be satisfied; although they are clearly not satisfied for the whole domain. However, as we have shown in a previous study [28, 30], the energy conditions should be evaluated by considering the complete set of Einstein equations. Thus, the observance of the energy conditions is much more subtle and must be treated with care.

Given that our geometric impositions are the same as warp drives, a system comparison is in order. In relation to that, a difference can be noted, as it has always been stated that for this type of spacetimes, the energy conditions are never satisfied. This can be seen in the Alcubierre metric and in more general ones like [51] where the WEC is always violated in the whole space domain. Moreover, it has been observed that for certain systems the NEC is always not fulfilled [14]. In contrast, in the system studied in this article, although the energy conditions are also violated in general, we can see for instance that there are space regions where the energy density is positive suggesting that by adding features to the material sector and making it more complex, there could be a path for a class of systems that does not fully violate the energy conditions.

In summary, we have found that by broadening the metric into considering the lapse function as an additional degree of freedom, it is possible to include heat flow within the matter content of the system. This, in turn, expands the modelling possibilities of the warp-based and potentially warp drive metrics and could therefore open up new avenues for theoretical explorations and developing applications.

We believe that it is essential to continue research into the different possibilities of the warp metric as well as the various ways to include different types of matter. This would be extremely useful not only for the complete understanding of warp theory and phenomenology but also for possible applications.

Data availability statement

No new data were created or analysed in this study.

Appendix

This appendix aims to give more details about method, the convergence, consistency and stability of the system of equations. The system of differential equations components obtained is

$$-\frac{\beta}{4\pi r\alpha^2}\frac{\partial\alpha}{\partial r}=q\,, \tag{51}$$

$$\frac{\beta}{r^2}\left(\beta+2r\frac{\partial\beta}{\partial r}\right)=8\pi\alpha^2\rho\,, \tag{52}$$

$$2r\alpha^2\frac{\partial\alpha}{\partial r}+2r\beta\left(\beta\frac{\partial\alpha}{\partial r}+\frac{\partial\alpha}{\partial t}\right)-\alpha\left(\beta^2+2r\beta\frac{\partial\beta}{\partial r}+2r\frac{\partial\beta}{\partial t}\right)=8\pi r^2\alpha^3 p_r\,, \tag{53}$$

$$\begin{aligned}&r\alpha^2\left(r\frac{\partial^2\alpha}{\partial r^2}-\frac{\partial\alpha}{\partial r}\right)+r\left(r\frac{\partial\beta}{\partial r}-\beta\right)\left(\beta\frac{\partial\alpha}{\partial r}+\frac{\partial\alpha}{\partial t}\right)\\&\quad+\alpha\left[\beta^2-r^2\beta\frac{\partial^2\beta}{\partial r^2}+r\left(\frac{\partial\beta}{\partial t}-r\left(\frac{\partial\beta}{\partial r}\right)^2-r\frac{\partial^2\beta}{\partial t\partial r}\right)\right]=8\pi r^2\alpha^3\Delta\,,\end{aligned} \tag{54}$$

with the constitutive relations (equations of state)

$$p_r=K_r\left(\rho-\lambda\right)\,, \tag{55}$$

$$\Delta=K_\Delta\left(\rho-\rho_0\right)\,. \tag{56}$$

Note that we are solving a system of six equations with six unknown functions, of which only α and β have explicit dynamics.

A.1. Consistency and stability of the numerical method

The consistency analysis of the numerical scheme section delves into the discretization of the Einstein equation components, specifically focusing on translating these components into a form suitable for numerical evaluation at discrete spatial and temporal points.

The discretized form of a specific Einstein equation component at a spatial point i and a temporal point n is shown by:

$$\begin{aligned}&2r_i\,\alpha_{i,n}^2\frac{\alpha_{i,n}-\alpha_{i-1,n}}{\Delta r}+2r_i\,\beta_{i,n}\left(\beta_{i,n}\frac{\alpha_{i,n}-\alpha_{i-1,n}}{\Delta r}+\frac{\alpha_{i,n}-\alpha_{i,n-1}}{\Delta t}\right)\\&\quad-\alpha_{i,n}\beta_{i,n}^2-2r_i\,\alpha_{i,n}\beta_{i,n}\frac{\beta_{i,n}-\beta_{i-1,n}}{\Delta r}\\&\quad-2r_i\,\alpha_{i,n}\frac{\beta_{i,n}-\beta_{i,n-1}}{\Delta t}-8\pi\,r_i^2\alpha_{i,n}^3K_r\left[\frac{\beta_{i,n}}{r_i^2}\left(\beta_{i,n}+2r_i\,\frac{\beta_{i,n}-\beta_{i-1,n}}{\Delta r}\right)\right]=0.\end{aligned} \tag{57}$$

This equation is then simplified to enhance the clarity of the numerical scheme's consistency analysis. The simplification process involves summarizing the effects of spatial and temporal discretization on the system's evolution. To accurately capture the derivatives, Taylor expansions are employed:

$$\frac{\alpha_{i,n}-\alpha_{i-1,n}}{\Delta r}=\left.\frac{\partial\alpha}{\partial r}\right|_{i,n}-\frac{\Delta r}{2}\left.\frac{\partial^2\alpha}{\partial r^2}\right|_{i,n}+\frac{\Delta r^2}{6}\frac{\partial^3\alpha}{\partial r^3}\left(\xi_r,n\right)+O\left(\frac{\partial^4\alpha}{\partial r^4}\right), \tag{58}$$

with similar expressions for β, showcasing the approach to approximating first and second-order derivatives in both space and time. The core of consistency analysis is encapsulated under the condition that the limit of the discretized equations approaches the original continuous equations as the discretization steps Δr and Δt approach zero. This analysis underscores

the scheme's ability to accurately represent the dynamics dictated by the continuous model, thereby ensuring that the numerical method is consistent with the theoretical underpinnings of the Einstein equations.

The consistency of a numerical scheme for solving differential equations, notably those derived from Einstein's equations, is predicated on the convergence of the discretized operator to the continuous operator as the discretization steps in space, Δr, and time, Δt, approach zero. This is formalized by the condition $Lu - Lu_{\mathrm{FD}} = 0$, which asserts that the error between the theoretical and numerical solutions diminishes with finer discretization.

The stability analysis of the MOL ensures that the solutions to the system of differential equations remain reliable. After employing the MOL and the Backward Euler method, a system of ordinary differential equations is formulated in the following generic form:

$$A\left(x^{n+1}\right)\left(x^{n+1}-x^{n}\right)=hF\left(x^{n+1}\right), \tag{59}$$

where x and F are vectors of size N with components that are given by the α_i and β_i, representing the number of spatial points, and A is an $N \times N$ matrix comprising the coefficient's of the system terms. h is used to denote the step size. It's assumed that A is invertible at any time t, leading to the global error representation E:

$$E_{n+1}=||A^{-1}\left(x^{n+1}\right)\left[A\left(x^{n+1}\right)\left(x_{ex}^{n+1}-x^{n+1}\right)\right]||. \tag{60}$$

which represents an expression that involves the difference between the exact solution x_{ex}^{n+1} and the numerical solution x^{n+1} at a given time step $n+1$. This equation is then adjusted to:

$$E_{n+1}=||A^{-1}\left(x^{n+1}\right)\left[A\left(x^{n+1}\right)x_{ex}^{n+1}-A\left(x^{n+1}\right)x^{n}-hF\left(x^{n+1}\right)\right]|| \tag{61}$$

further refining the expression for the global error. Using the property of norms in R^m, the error can be expanded and estimated as follows:

$$\begin{aligned}E_{n+1}\leqslant\ & ||A^{-1}\left(x^{n+1}\right)\left[A\left(x^{n+1}\right)x_{ex}^{n}-A\left(x^{n+1}\right)x^{n}\right]|| \\ & +||A^{-1}\left(x^{n+1}\right)h\left[F\left(x_{ex}^{n+1}\right)-F\left(x^{n+1}\right)\right]|| \\ & +||A^{-1}\left(x^{n+1}\right)\left[A\left(x^{n+1}\right)x_{ex}^{n+1}-A\left(x^{n+1}\right)x_{ex}^{n}-hF\left(x_{ex}^{n+1}\right)\right]||.\end{aligned} \tag{62}$$

The stability of a numerical scheme can be quantitatively described by bounding the global error E_{n+1}, expressing how the error at the next time step E_{n+1} is related to the error at the current time step E_n, considering the step size h. This is found by obtaining bounds for the function matrix A by proving that it is Lipschitz continuous; that is, if there exists a constant L, known as the Lipschitz constant, satisfying

$$|f(x_1)-f(x_2)|\leqslant L|x_1-x_2|,$$

for any two points x_1 and x_2 within that domain. This condition ensures that the function's rate of change is bounded by L, offering a constraint on the function's first derivative across the domain. After a long proof, $A(x)$ is found to be Lipschitz continuous, then

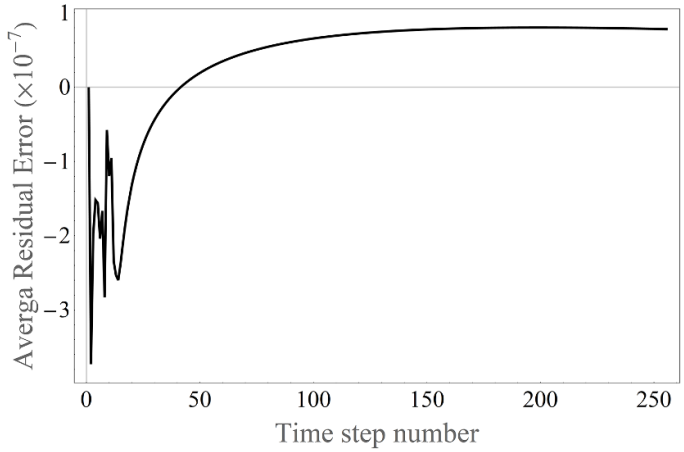

Figure 8. Evolution of the average residual over time steps, demonstrating the numerical solver's convergence.

$$
\begin{aligned}
||A\left(x_{ex}^{n+1}\right) - A\left(x^{n+1}\right)|| &= \sum_{i=1}^{N}\sum_{j=1}^{N} |a_{ij}\left(x_{ex}^{n+1}\right) - a_{ij}\left(x^{n+1}\right)| \\
&\leqslant \sum_{i=1}^{N}\sum_{j=1}^{N} L_{ij}||x_{ex}^{n+1} - x^{n+1}|| \\
&\leqslant L_{A0}\sum_{i=1}^{N}\sum_{j=1}^{N} ||x_{ex}^{n+1} - x^{n+1}|| \\
&= L_{A0}N^2||x_{ex}^{n+1} - x^{n+1}|| \,, \qquad (63)
\end{aligned}
$$

where L_{ij} are the Lipschitz constants of $a_{ij}(x)$ and $L_{A0} = \max(L_{ij})$. Now putting $L_A = L_{A0}N^2$

$$
||A\left(x_{ex}^{n+1}\right) - A\left(x^{n+1}\right)|| \leqslant L_A||x_{ex}^{n+1} - x^{n+1}|| = L_A E_{n+1} \,. \qquad (64)
$$

After including the previous inequalities and some large calculation, we find that,

$$
E_{n+1} \leqslant \exp\left(T_f a\right) E_0 + \exp\left(T_f a\right) \frac{Mh}{2a}
$$

where $T_f a$ represents the final time up to which the simulation or numerical method is run and $x_{ex}''(t_e) = M$. This implies that the error goes to zero as the time step h goes to zero.

In figure 8, the error analysis involves the calculation of residuals (the difference between the left-hand side and the right-hand side of an equation, given a current approximation in the PETs package) from the fundamental equations at every point in the spatial domain. To obtain a measure of error that is comparable across different scenarios, the sum of these residuals is normalized by the total number of equations, which corresponds to twice the number of spatial points due to the dual equations evaluated at each point.

The process begins with the computation of residuals for each of the equations, reflecting the current discrepancy from the true solutions. These residuals are then summed across the spatial domain to gauge the overall error at a given time step. By dividing this sum by the total number, an average residual is obtained, offering a standardized metric of error per equation.

Tracking the average residuals over successive time steps provides information on the convergence behaviour of the solver. A decrease in the average residual indicates an improvement in the performance of the solver.

ORCID iD

G Abellán https://orcid.org/0000-0001-5968-9840

References

[1] Alcubierre M 1994 *Class. Quantum Grav.* **11** L73–L77
[2] Olum K D 1998 *Phys. Rev. Lett.* **81** 3567–70
[3] Pfenning M J 1998 Quantum inequality restrictions on negative energy densities in curved spacetimes (arXiv:gr-qc/9805037)
[4] Low R J 1999 *Class. Quantum Grav.* **16** 543–9
[5] Van Den Broeck C 1999 arXiv:gr-qc/9906050
[6] Barcelo C and Visser M 2000 *Class. Quantum Grav.* **17** 3843–64
[7] Lobo F and Crawford P 2003 *Current Trends in Relativistic Astrophysics* (*Lecture Notes in Physics* vol 617) (Springer) pp 277–91
[8] Barcelo C and Visser M 2002 *Int. J. Mod. Phys.* D **11** 1553–60
[9] Lobo F S N and Visser M 2004 *Class. Quantum Grav.* **21** 5871–92
[10] McMonigal B, Lewis G F and O'Byrne P 2012 *Phys. Rev.* D **85** 064024
[11] Alcubierre M and Lobo F S N 2017 *Wormholes, Warp Drives and Energy Conditions* (*Fundamental Theories of Physics* vol 189) (Springer) pp 257–79
[12] Alcubierre M and Lobo F S N 2017 *Wormholes, Warp Drives and Energy Conditions* vol 189 (Springer)
[13] Lentz E W 2021 *Class. Quantum Grav.* **38** 075015
[14] Santiago J, Schuster S and Visser M 2022 *Phys. Rev.* D **105** 064038
[15] Hiscock W A 1997 *Class. Quantum Grav.* **14** L183–8
[16] Clark C, Hiscock W A and Larson S L 1999 *Class. Quantum Grav.* **16** 3965–72
[17] Gonzalez-Diaz P F 2000 *Phys. Rev.* D **62** 044005
[18] Everett A E 1996 *Phys. Rev.* D **53** 7365–8
[19] Arnowitt R L, Deser S and Misner C W 2008 *Gen. Relativ. Gravit.* **40** 1997–2027
[20] Wald R M 1984 *General Relativity* (Chicago University Press) (https://doi.org/10.7208/chicago/9780226870373.001.0001)
[21] Alcubierre M 2008 *Introduction to 3+1 Numerical Relativity* (Oxford Academic) (https://doi.org/10.1093/acprof:oso/9780199205677.001.0001)
[22] Santos-Pereira O L, Abreu E M C and Ribeiro M B 2020 *Eur. Phys. J.* C **80** 786
[23] Santos-Pereira O L, Abreu E M C and Ribeiro M B 2021 *Eur. Phys. J. Plus* **136** 902
[24] Santos-Pereira O L, Abreu E M C and Ribeiro M B 2021 Warp drive dynamic solutions considering different fluid sources *16th Marcel Grossmann Meeting on Recent Developments in Theoretical and Experimental General Relativity, Astrophysics and Relativistic Field Theories*
[25] Santos-Pereira O L, Abreu E M C and Ribeiro M B 2021 *Gen. Relativ. Gravit.* **53** 23
[26] Santos-Pereira O L, Abreu E M C and Ribeiro M B 2021 *Eur. Phys. J.* C **81** 133
[27] Bobrick A and Martire G 2021 *Class. Quantum Grav.* **38** 105009
[28] Abellan G, Bolivar N and Vasilev I 2023 *Eur. Phys. J.* C **83** 7
[29] Abellán G, Bolívar N and Vasilev I 2023 Warp drive solutions in spherical coordinates with anisotropic matter configurations (arXiv:2305.03736)
[30] Abellan G, Bolivar N and Vasilev I 2023 *Gen. Relativ. Gravit.* **55** 60
[31] Thorne K S and MacDonald D 1982 *Mon. Not. R. Astron. Soc.* **198** 339
[32] Tolman R C 1934 *Relativity, Thermodynamics and Cosmology* (Dover Publications)
[33] Volovik G E 2019 *JETP Lett.* **109** 8–11
[34] Herrera L and Santos N O 1997 *Phys. Rep.* **286** 53–130
[35] Rosenhauer A, Staubo E F, Csernai L P, Øvergård T and Østgaard E 1992 *Nucl. Phys.* A **540** 630–45
[36] Dalcin L D, Paz R R, Kler P A and Cosimo A 2011 *Adv. Water Resour.* **34** 1124–39

[37] Ti-petsc - an interface to petsc from titanium (available at: www.nersc.gov/˜yunhe/cs267/final/paper.pdf)
[38] Brown J, Le Pourhiet L, May D A and Sanan P 2018 PTatin3D (available at: https://bitbucket.org/jedbrown/ptatin3d)
[39] Balay S et al 2023 PETSc/TAO users manual *Technical Report* (ANL-21/39 Revision 3.20 Argonne National Laboratory)
[40] Visser M 1995 *Lorentzian Wormholes: From Einstein to Hawking* (American Institute of Physics Melville)
[41] Poisson E 2004 *A Relativist's Toolkit : The Mathematics of Black-Hole Mechanics* (Cambridge University Press) (https://doi.org/10.1017/CBO9780511606601)
[42] Carroll S M 2004 *Spacetime and Geometry: An Introduction to General Relativity* (Cambridge University Press) (https://doi.org/10.1017/9781108770385)
[43] Curiel E 2017 *Towards a Theory of Spacetime Theories* (*Einstein Studies* vol 13) (Birkhäuser) pp 43–104
[44] Kontou E A and Sanders K 2020 *Class. Quantum Grav.* **37** 193001
[45] Hawking S W and Ellis G F R 2023 *The Large Scale Structure of Space-Time* (*Cambridge Monographs on Mathematical Physics*) (Cambridge University Press)
[46] Kolassis C, Santos N and Tsoubelis D 1999 *Class. Quantum Grav.* **5** 1329
[47] Maeda H and Martinez C 2020 *Prog. Theor. Exp. Phys.* **2020** 043E02
[48] Maeda H and Harada T 2022 *Class. Quantum Grav.* **39** 195002
[49] Martin-Moruno P and Visser M 2018 *Class. Quantum Grav.* **35** 125003
[50] Reboucas M J and Tiomno J 1983 *Phys. Rev.* D **28** 1251–64
[51] Natário J 2002 *Class. Quantum Grav.* **19** 1157–66